



Full Length Article

Probing of O₂ vacancy defects and correlated magnetic, electrical and photoresponse properties in indium-tin oxide nanostructures by spectroscopic techniques

Shyamsundar Ghosh^{a,*} Bhupendra Nath Dev^b

^a Department of Physics, Bejoy Narayan Mahavidyalaya (affiliated to The University of Burdwan), P. O. Itachuna, Hooghly 712 147, India

^b Department of Material Science, Indian Association for the Cultivation of Science, 2A & 2B Raja S. C. Mullick Road, Jadavpur, Kolkata 700 032, India

ARTICLE INFO

Article history:

Received 22 May 2017

Revised 27 December 2017

Accepted 8 January 2018

Available online 11 January 2018

Keywords:

ITO nanostructures

Oxygen vacancy

Ferromagnetism

Photoluminescence

Photoresponse

ABSTRACT

Indium-tin oxide (ITO) 1D nanostructures with tunable morphologies i.e. nanorods, nanocombs and nanowires are grown on c-axis (0 0 0 1) sapphire (Al₂O₃) substrate in oxygen deficient atmosphere through pulsed laser deposition (PLD) technique and the effect of oxygen vacancies on optical, electrical, magnetic and photoresponse properties is investigated using spectroscopic methods. ITO nanostructures are found to be enriched with significant oxygen vacancy defects as evident from X-ray photoelectron and Raman spectroscopic analysis. Photoluminescence spectra exhibited intense mid-band blue emission at wavelength of region of 400–450 nm due to the electronic transition from conduction band maxima (CBM) to the singly ionized oxygen-vacancy (V_O[•]) defect level within the band-gap. Interestingly, ITO nanostructures exhibited significant room-temperature ferromagnetism (RTFM) and the magnetic moment found proportional to concentration of V_O[•] defects which indicates V_O[•] defects are mainly responsible for the observed RTFM in nanostructures. ITO nanowires being enriched with more V_O[•] defects exhibited strongest RTFM as compared to other morphologies. Current voltage (I-V) characteristics of ITO nanostructures showed an enhancement of current under UV light as compared to dark which indicates such 1D nanostructure can be used as photovoltaic material. Hence, the study shows that there is ample opportunity to tailor the properties of ITOs through proper defect engineering's and such photo-sensitive ferromagnetic semiconductors might be promising for spintronic and photovoltaic applications.

© 2018 Elsevier B.V. All rights reserved.

1. Introduction

The study of defect-induced *d*⁰ ferromagnetism in various low-dimensional (1D/2D) metal-oxide nanostructures and thin-films has been drawn immense research attentions for novel spintronic and opto-spintronic applications [1,2]. The discovery of room temperature ferromagnetism (RTFM) in pure HfO₂ thin films [3] demonstrates an interesting physics indicating that the oxide semiconductors can exhibit FM without the presence of any d or f-electrons. Although, scientists have primarily attempted to prepare oxide-based dilute magnetic semiconductors [4–11] by dilute doping of transition metal ions (Co, Mn, Fe etc.) within semiconducting host. However, the magnetic properties of such transition-metal-doped O-DMSs remain quite controversial [4–11] still to date. On the other hand, reducing size or dimension of the material to nanosize (~10⁻⁹ m) scale, it is often advantageous to

enhance many physical properties like optical, magnetic and electrical properties [12,13]. Such low-dimensional (1D/2D) nanostructures in the form of nanowires, nanorods and thinfilms are generally prone to be enriched with many surface defects, oxygen and cation vacancies [14–16] due to their low formation energy within nanoscale materials. The RTFM was reported in the pristine ZnO, TiO₂, In₂O₃ and SnO₂ nanostructures and thinfilms [6–11,15–18]. The origin of FM has been attributed to the different structural defects present in these oxide semiconductors. Based on the ab initio calculations for HfO₂ and CaO, Pemmaraju et al. [6] and Elfimov et al. [7] indicated that the cation vacancies can induce an almost localized magnetic moment on the oxygen atoms neighboring the vacancy. On the other hand, oxygen vacancies (V_O) have also been attributed to introducing RTFM in wide-band-gap oxide semiconductors such as ZnO, SnO₂ [3,8,10,18].

Sn-doped In₂O₃, commonly known as indium-tin oxide (ITO) is a promising n-type wide-bandgap (~3.5 eV) transparent metal-oxide semiconductor having high electrical conductivity and generally finds potential technological applications in solar cells, light

* Corresponding author.

E-mail address: sghoshphysics@gmail.com (S. Ghosh).

emitting diodes, liquid crystal displays, gas sensors and photovoltaic cells [19–21], etc. During the growth of ITO nanostructures in variable condition, formation of different intrinsic crystal defects such as In interstitials, oxygen vacancy (V_O), and In vacancy (V_{In}) can occur within ITO lattice. However, it is unlikely to have significant amount of V_{In} defects without proper defect engineering due to the high formation energy of V_{In} . On contrary, oxygen vacancy (V_O) can stabilize easily due to its low formation energy specially in oxygen-deficient atmosphere. However, still date, there are limited numbers of reports on the defect-related magnetic properties of ITO nanostructures. Not only magnetic properties but optical properties also found to depend strongly on inherent crystalline defects. Peng et al. [22] have shown that the origin of photoluminescence in indium oxide is due to presence of oxygen vacancies while Kumar et al. [23] reported the indium interstitials and associated complex defects are responsible for the photoluminescence in In_2O_3 . However, the formation of such defects strongly depends on crystal growth condition and nanostructure morphology [24]. Therefore, a correlated study of magnetic, optical and electrical properties in such 1D nanostructure of Sn-doped In_2O_3 would be convenient in order to understand the physical properties in low-dimension limit.

In this article, various ITO nanostructures in the form of nanorods (NRs), nanocombs (NCs) and nanowires (NWs) have been fabricated on c-axis (0 0 0 1) Al_2O_3 substrate in oxygen-deficient atmosphere through pulsed laser deposition (PLD). ITO nanostructures found to exhibit significant FM and visible photoluminescence at RT. Evidence of oxygen vacancy formation has been confirmed employing various spectroscopic techniques and it is found singly charged/ionized oxygen vacancies (V_O^\bullet) are responsible for such RTFM and PL. Effect of photon illumination on current-voltage (I-V) characteristics of ITO nanostructures are also investigated and they exhibited excellent photoresponse in UV-visible light. It has also been found that among the various morphologies, 1D ITO NWs exhibited strongest RTFM, superior photoluminescence with excellent photoresponse due to presence of more oxygen vacancies or surface defects. Hence, the possibility of tailoring RTFM in oxide-based semiconductors through proper defect engineering can open new horizons in the field of spintronics.

2. Experimental details

2.1. Synthesis and characterization of nanostructures

ITO nanostructures with tunable morphologies are fabricated on the c-axis (0 0 0 1) sapphire (Al_2O_3) substrate using pulsed laser deposition (PLD) unit with a KrF excimer laser with following specifications: (i) laser power density $\sim 1.41 \text{ J/cm}^2$, (ii) the pulse repetition rate 5 Hz and (iii) substrate temperature 600°C . At first, high purity (99.998%) In_2O_3 and SnO_2 powders mixed properly with appropriate ratio (In:Sn = 9:1) and grinded well to prepare a uniform mixture. The target was prepared from the mixture in the form of a pallet of 1 inch diameter and sintered in air at 800°C for 5 h. Then the target was mounted within the PLD chamber which was evacuated down to atmospheric pressure of 2×10^{-3} Pascal. Then, pure argon (Ar) gas was pushed into the chamber and three different ITO samples were prepared at three different Ar pressure such as 1, 10 and 100 Pascal (Pa). The deposition process was continued for 30 min and then the sample was annealed for 10 min in the same atmosphere and then cooled naturally at room temperature.

The samples are characterised by Grazing Incidence X-ray Diffraction (GIXRD, X'Pert Pro, Panalytical) to estimate the crystal structure, phase and lattice parameters of the ITO unit cell. Field

Emission Scanning Electron Microscopy (FESEM, FEI Helios Nanolab-600) was used to observe the morphology and growth of the nanostructures. The chemical composition, valence state of the ions and presence of intrinsic defects was analyzed from X-ray photoelectron spectroscopy (XPS, PHI 5000 Versaprobe II Scanning XPS microprobe, ULVAC-PHI, USA) at RT with a monochromatic Al K_{α} ($h\nu = 1486.6 \text{ eV}$) radiation. Photoluminescence (PL) spectroscopic measurement was performed to observe the band to band transition and defect level transition within the energy band-gap of ITOs using a spectrofluorometer (Horiba Jobin Yvon, Fluorolog-3) a Xe lamp source under the excitation wavelength of 330 nm. Raman spectroscopy measurements were carried out using a micro-Raman spectrometer (LABRAM HR from Horiba Jobin Yvon) at RT. Magnetic measurements are performed by superconducting quantum interference devices (SQUIDs). Hall measurements performed to estimate the type of electrical conductivity and carrier concentration of ITO nanostructures. Current-voltage characteristics of the ITO nanostructures are measured using a four-probe method using a constant current source and a nanovoltmeter under both dark and ultra-violet (UV) light using an UV lamp of 200 W power.

3. Results and discussions

3.1. Morphology and crystal structure

Field emission scanning electron microscopy (FESEM) is employed to observe the morphology of the ITO samples and it is seen that the presence of oxygen deficient Ar atmosphere during the deposition process is found to have significant effect on the growth, morphology and dimension of ITOs. Fig. 1a–c shows the FESEM micrographs of ITOs prepared under Ar pressure of 1 Pa. From the figure, it is evident that the ITO deposited at relatively low Ar pressure (i.e. at 1 Pa) is found have mainly vertical rod-like morphology with blunt-tip, called ITO nanorods (NRs). The appearance of big ball-like structures, as can be seen from Fig. 1a, indicates they were formed by the vapor-liquid-solid (VLS) growth mechanism [25]. During deposition at high temperature, both In and Sn vapour reach on substrate where they can form In–Sn alloy droplet. This In–Sn alloy droplet can act as nuclei for VLS growth of ITO nanorods or nanowires [26]. Frank et al. [26] showed that both In_2O_3 and SnO_2 can be dissolved into In–Sn alloy droplet and form In–Sn–O (In:Sn = 9:1) ternary alloy melts. In an oxygen deficient atmosphere at high temperature, In_2O_3 :Sn nanocrystals will be grown in specific direction from metallic In–Sn–O alloy droplets [25], as evident as the big ball-like structures in Fig. 1a. Similar results also reported by Chen et al. [26] in which bulk-quantity ITO nanowires were synthesized by direct thermal evaporation in air at 920°C of a mixture of In and SnO powders.

When the Ar pressure is increased to 10 Pa, the entire ITO sample is found to contain only large number of distinct comb-like nanostructures, can be called ITO nanocombs (NCs) as shown in Fig. 1d–f. An ITO nanocomb consists of a solid nano-stem, having average diameter ~ 70 – 80 nm , and perpendicular rod-like branches with ~ 40 – 50 nm diameters coming out of the stem. The disappearance of the spherical particles in the film indicates a decrease in the amount of liquid material present during growth. The nanowires and their branches are longer than the ones formed at lower pressure, since the material that was present in the big structures is now used to form the wires. This seems to be reasonable if we assume that the amount of material reaching the substrate is approximately the same for both depositions. On further increase of Ar pressure to 100 Pa, ITO samples is found to consist of only large number of long (about a few μm) ITO nanowires (NWs) as shown in Fig. 1g–i. The diameter of the individual

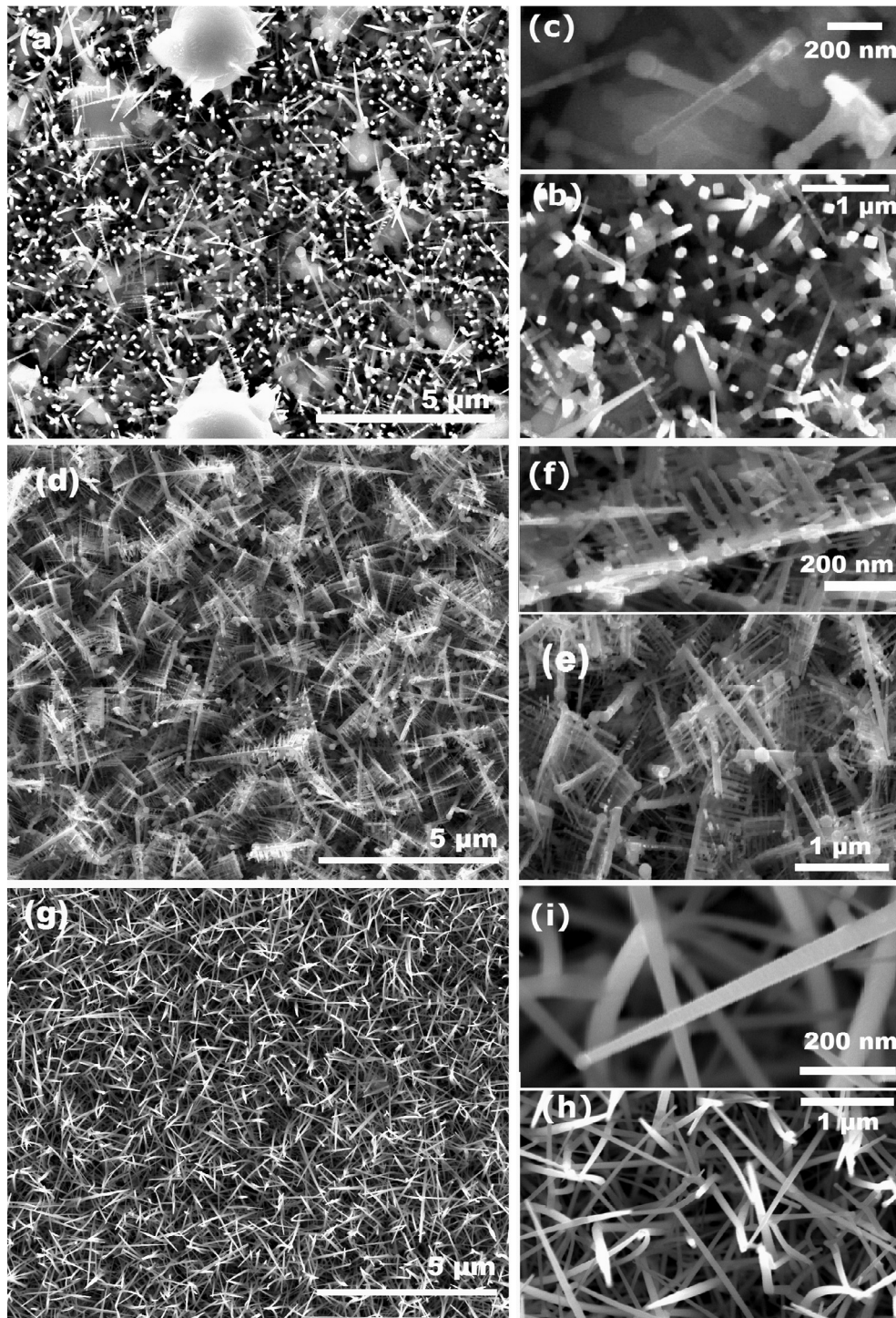


Fig. 1. FESEM images of ITO Nanorods (a–c), Nanocombs (d–f) and Nanowires (g–i) prepared at Ar pressure of 1, 10 and 100 Pascal (Pa) respectively.

nanowire is found to vary from ~ 30 to 80 nm along the length of the nanowire. Careful observation shows the appearance of tiny ball on the tip of each nanowire which again supports the vapor-liquid-solid (VLS) growth mechanism [25,26] as stated earlier.

Fig. 2a shows the X-ray diffraction pattern of the ITO nanostructures that exhibit two major diffraction peaks from (2 2 2) and (4 0 0) plane. It indicates a cubic bixbyite crystal structure (JCPDS#17-2195) of indium oxide. The estimated lattice parameter 'a' of the cubic ITO structure is found to increase with increasing Ar pressure which suggests an expansion of unit cell. A ratio of intensities

$[I_{(400)}/I_{(222)}]$ for (4 0 0) and (2 2 2) diffraction peaks are also estimated and plotted against the Ar pressure in Fig. 2b. A high ratio is obtained for ITO NWs which was deposited at 100 Pa Ar pressure, indicates that the NWs are highly orientated along [4 0 0] direction. With the decrease of Ar pressure, the degree of orientation decreases initially for comb-like nanostructures and then again increases little bit for the rod-like nanostructures. For the ITO NCs, the degree of orientation along [4 0 0] direction diminishes because the individual nanorod possess many perpendicular branches.

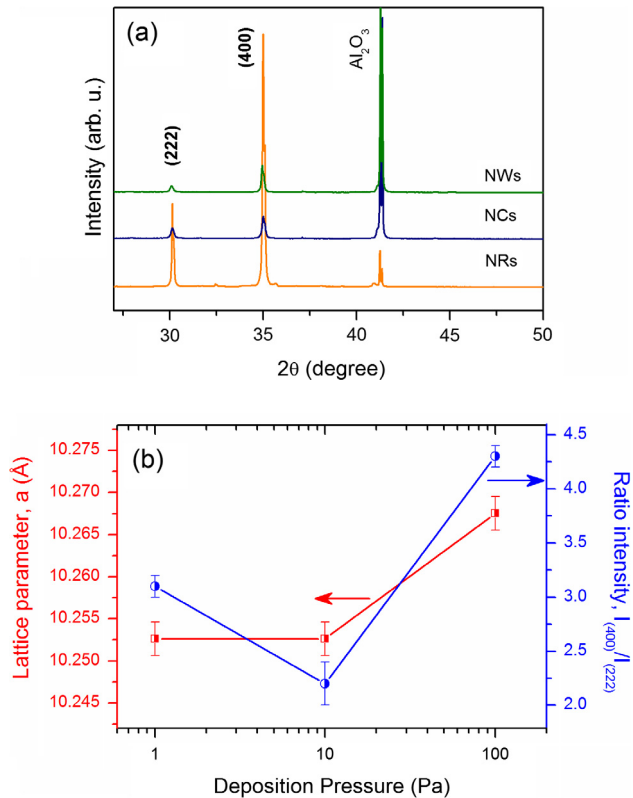


Fig. 2. (a) X-ray diffraction pattern of ITO nanostructures, (b) variation of lattice parameter of cubic ITO unit cell and the ratio intensity of (400) and (222) diffraction peak with the deposition (Ar) pressure.

3.2. X-ray photoelectron spectroscopy studies

XPS is known to be very effective tool to study the valence state of the ions as well as surface defects in nanostructures. Fig. 3 shows the core level XPS spectra of (a) In 3d and (b) O 1s of the ITO nanostructures. Due to the broad and asymmetric nature of the peak, each peak of In 3d can be fitted in two peaks with different intensities and position. The pair of peaks located at 445.5 and 453.1 eV (with energy difference $\Delta E = 7.6$ eV) correspond to In 3d_{5/2} and 3d_{3/2} orbitals for In³⁺ oxidation state in ITOs [27,28]. Two other pair of peaks with smaller intensities located at 444.6 eV and 452.2 eV (with $\Delta E = 7.6$ eV) correspond to In 3d_{5/2} and 3d_{3/2} orbitals, respectively for the metallic In state (In⁰) [27]. This suggests that within the ITO nanostructures, indium should be present in lower oxidation state too. This result indicates that In³⁺ ions surrounded by oxygen vacancies might occupy electrons from the oxygen vacancy cavity and transform to metallic In introducing a singly charged oxygen vacancy (V_{O}^{\bullet}) defects in ITO matrix. XPS spectra of Sn 3d core level for ITOs (at inset of Fig. 3a) exhibits two distinct peaks at 486.4 and 494.9 eV corresponding to Sn 3d_{5/2} and 3d_{3/2} orbitals, respectively, indicating that the dopant Sn is in 4+ oxidation state [27]. O 1s core level spectra (Fig. 3b) can also be deconvoluted into two peaks centred at 530.5 and 532 eV respectively. The peak with lower binding energy (i.e. at 530.5 eV) corresponds to lattice oxygen in crystalline ITO and higher one (at 532 eV) is associated with the oxygen vacancy defects in lattice [29,30]. It can be seen from the figure that with the increase of Ar pressure, the gradual broadening of the spectra towards higher energy side demonstrates the formation of more oxygen vacancy within lattice and thus the ITO NWs (prepared at 1 mbar Ar pressure) contain more oxygen vacancy defects compared to the other morphologies.

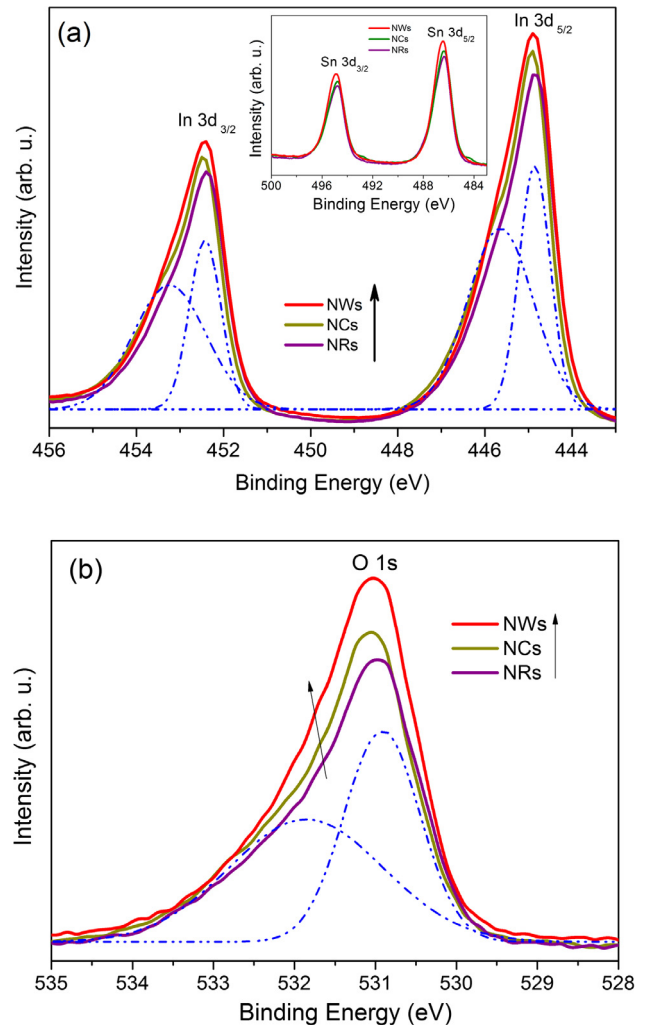


Fig. 3. XPS spectra of (a) In 3d, Sn 3d (inset) and (b) O 1s core-level of the ITO nanostructures.

3.3. Photoluminescence properties

Evidence of oxygen vacancy formation is also confirmed from the room-temperature photoluminescence spectra of ITO nanostructures, as shown in Fig. 4. It is interesting to notice that the ITOs exhibit several intense mid-band blue/blue-green emissions (Fig. 4a) along with weak UV emission. The individual PL spectra for NRs (Fig. 4b), NCs (Fig. 4c) and NWs (Fig. 4d) can be well fitted into five different emission peaks located at 354 (peak 1), 387 (peak 2), 415 (peak 3), 436 (peak 4) and 500 (peak 5) nm. UV emission (peak1) of the ITOs is believed to be because of the near band edge (NBE) radiative transitions due to the photogenerated electrons [31,32]. The emission near 387 nm (peak 2) is related to the defect-level/state introduced into the band gap of ITO because of the Sn doping as they introduce shallow trap state [31]. Besides this, all ITOs are found to exhibit significant blue/blue-green (400–500 nm) regions, which are believed to be because of the various crystalline defects, surface defects and different oxygen vacancy defects such as V_{O}^{2+} (doubly charged), V_{O}^{\bullet} (singly charged) and V_{O} (neutral) [22,31,33]. The emission peak in blue region located at 415 nm (peak 3) can be ascribed to the deep level singly charged oxygen vacancies (V_{O}^{\bullet}), also known as F^+ centre defects [22,31,34], whereas the emission band at 436 nm (peak 4) can be due to other type of oxygen vacancies. It can be seen from Fig. 4a

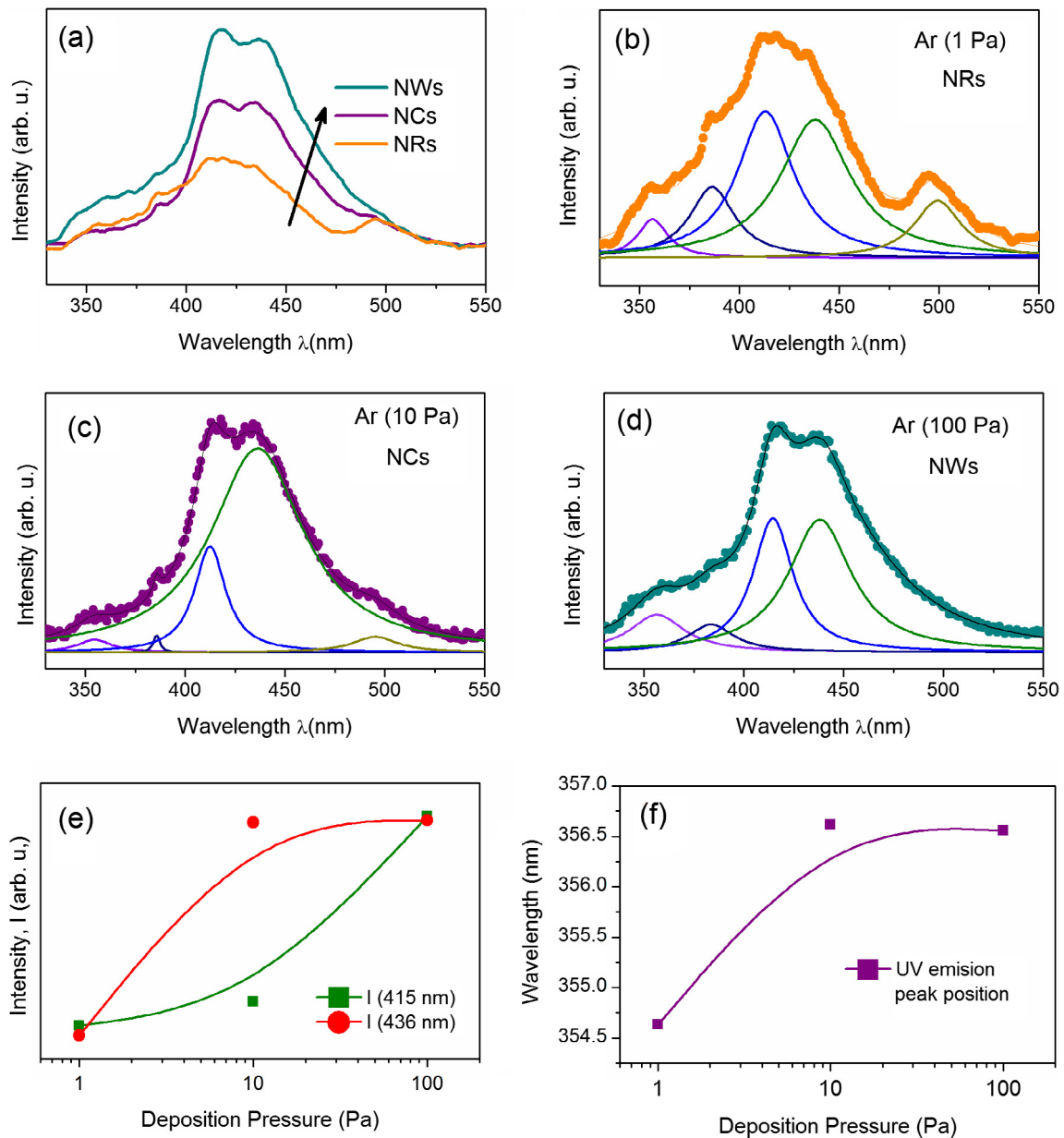


Fig. 4. Photoluminescence spectra of (a) ITO nanostructures with different morphology. Individual PL spectra for ITO (b) NRs (c) NCs and (d) NWs with the corresponding fitted peaks. (e) Variation of intensities of the two blue emission peaks (located at 415 and 436 nm) with deposition pressure. (f) Redshift of UV emission peak with deposition pressure. (For interpretation of the references to colour in this figure legend, the reader is referred to the web version of this article.)

that with the increase of deposition pressure, the intensity of defect emission at blue-green region increases gradually and the ITO NWs exhibits most intense defect emission bands compared to the other ITO morphologies. The relative intensity of defect-emission Peak 3 (415 nm) and Peak 4 (436 nm) for all the ITO morphologies are plotted with Ar pressure and shown in Fig. 4e. The increase of intensities of these two blue emission peaks indicates that the concentration of V_O defects increases monotonically and ITO NWs possess highest amount of V_O defects. Due to the loss of an O atom from ITO lattice, the electron pair that remains trapped in the oxygen vacancy cavity (V_O) give rise to an F centre defect [35]. One of the electrons in F centre is likely to occupy the neighboring In^{3+} ion (as the matrix is mostly richer with In) and generates a F^+ centre defects within the band-gap of ITO. The redshift of UV emission peak (Fig. 4f) might be due to incorporation of various defects levels within the energy band-gap of ITO.

3.4. Raman spectroscopy studies

Raman spectroscopy is also employed to probe various bending and stretching vibrational levels and also probe the oxygen vacancy defects within ITO lattice. The cubic bixbyite structure of ITO is expected to exhibit 22 Raman active and 16 infrared active modes, however only 6 Raman active modes has been observed in pure cubic single crystalline In_2O_3 and ITO nanostructures [36]. The Raman spectra of ITO nanostructures as shown in Fig. 5 show 6 Raman modes at 103, 130, 306, 363, 499 and 612 cm^{-1} , which compares well with those observed in literature [36]. The Raman mode at 130 cm^{-1} for ITOs is ascribed to the In–O vibrations of InO_6 octahedra [36]. The 306 and 499 cm^{-1} modes are demonstrated as the bending and stretching vibrations of InO_6 octahedra, respectively. In In_2O_3 , 366 cm^{-1} peak is assigned to the stretching vibrations of the In–O–In in the unit cell of ITO. It

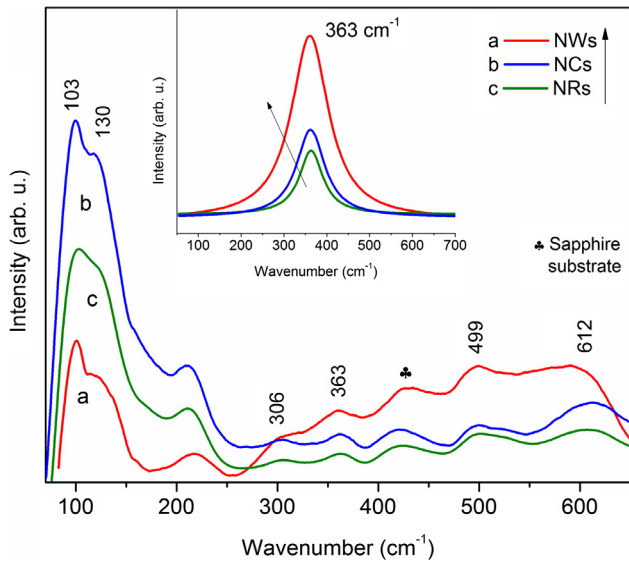


Fig. 5. Raman spectra of the ITO nanostructures with different morphologies; Inset: Redshift of 363 cm^{-1} Raman active mode with change in morphology.

is found that the vibration of In—O—In bond is greatly affected by the presence of V_o defects. The change in intensity and shifting of Raman peak position is caused by such defects. Hence, the observed red shift of mode of In—O—In vibrations to 363 cm^{-1} for the ITOs can be attributed to the weaker binding forces due to creation of oxygen vacancies. Since the most dominant part in the Raman scattering intensity is proportional to the square of the derivative of the polarizability to the amplitude the normal mode, creation of oxygen vacancies are expected to change the intensity of 363 cm^{-1} Raman mode. The inset of Fig. 5 shows the fitted Gaussian plots corresponding to 363 cm^{-1} Raman active mode for different nanostructure morphology and the peak position found to be 363.5 , 362.1 and 360.5 cm^{-1} for NRs, NCs and NRs respectively. This redshift and increase of intensity of 363

cm^{-1} peak demonstrates the NWs contain more oxygen vacancies [36] compared to other morphologies.

3.5. Electrical and magnetic properties

Fig. 6 shows the variation of electrical resistivity (ρ), carrier concentration (η) and carrier mobility (μ) for the ITOs with deposition pressure. With the increase of Ar pressure, the value of ' ρ ' decreases while ' η ' and ' μ ' increases gradually. Thus the ITO NWs exhibits lowest value of ' ρ ' ($\sim 4 \times 10^{-4}\ \Omega\text{ cm}$) and highest ' η ' $\sim 6.4 \times 10^{20}\text{ cm}^{-3}$. This is because ITO NWs possess the highest amount of V_o defects, as evident from earlier studies and thus raises n-type carrier (electron) concentration [37,38]. With the decrease of Ar pressure, the concentration of the V_o defects decreases in the respective morphologies, thus carrier (electron) concentration decreases, consequently an increase of resistivity. Magnetic properties of the ITO nanostructures are measured using SQUID magnetometer at room temperature. Interestingly, the ITO nanostructures are found to exhibit significant room-temperature ferromagnetism (RTFM). Fig. 7a shows the magnetization hysteresis (M-H) loop of the ITO nanostructures at RT. It is evident that the ITOs exhibit ferromagnetic behavior with well-defined coercivity (H_c) and saturation magnetization (M_s). The temperature-dependent magnetization (M-T) curve in Fig. 7b shows the Curie temperature (T_c) of ITO nanostructures are well above RT. As the deposition pressure in PLD increases, both M_s and T_c are found to increase gradually. Among the different morphologies, ITO NWs exhibits strongest ferromagnetism (FM) with $M_s \sim 23.5\text{ emu/cm}^3$ and $T_c \sim 468\text{ K}$.

Such RTFM has also been observed in other low dimensional oxide semiconductors, where the origin of FM was ascribed to several point defects [15–18]. It has been found that the cation (In) vacancy and oxygen vacancy can introduce local magnetic moment and ferromagnetic interaction between the magnetic defects can be mediated through the charge carriers [39,40]. However, here we have not found any evidence of formation of In vacancy in these ITO nanostructures. On the other hand, the observation of higher energy peak at 532 eV in O 1s core-level XPS, blue emission in PL

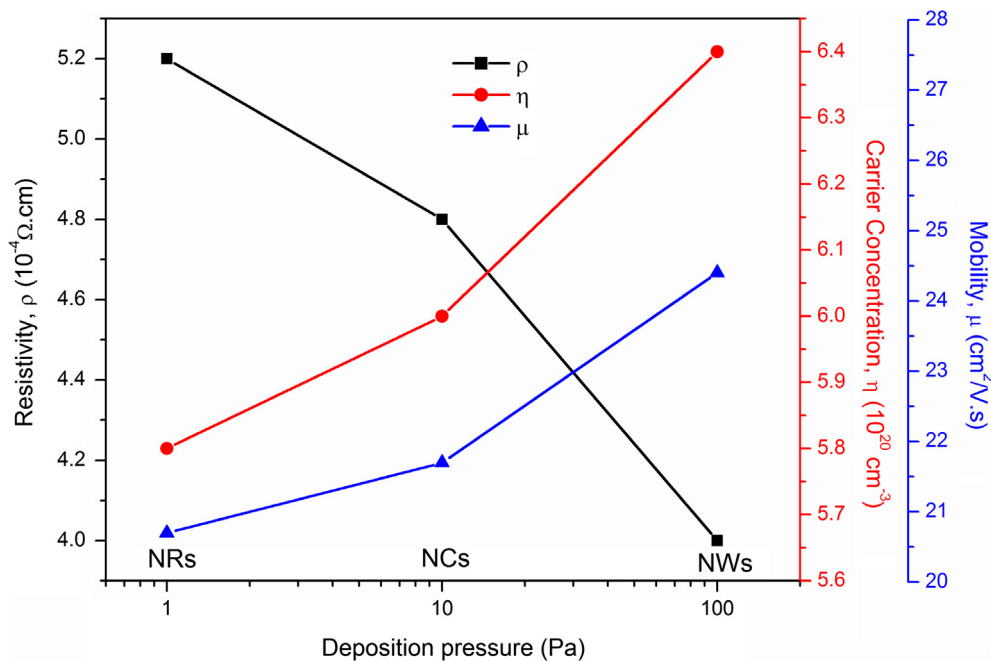


Fig. 6. Variation of electrical resistivity, carrier concentration and mobility of the ITO nanostructures with deposition pressure.

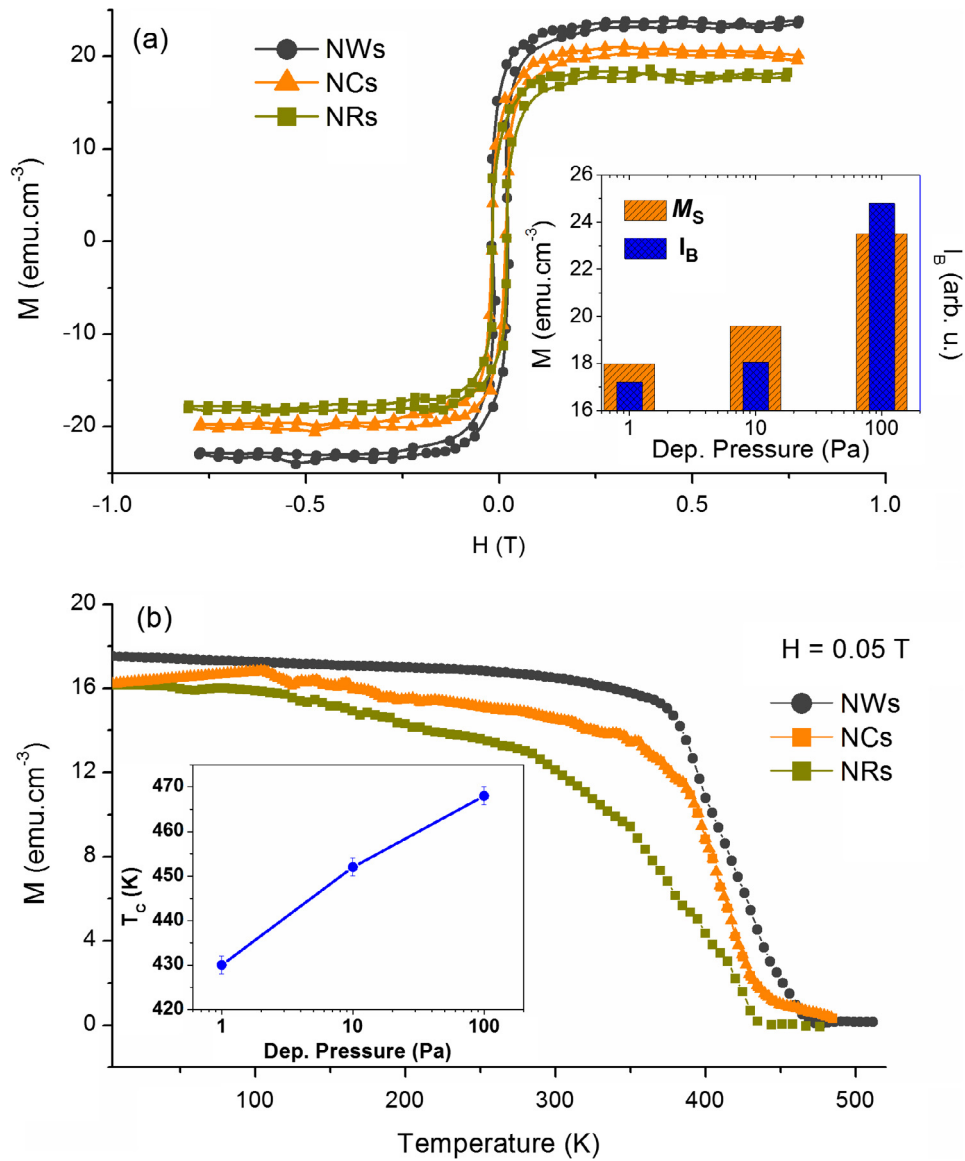


Fig. 7. (a) Magnetic hysteresis (M-H) loop of ITO nanostructures. Inset: Correlated variation of M_S and corresponding PL blue emission (located at 415 nm) intensity (I_B) with deposition pressure. (b) Temperature-dependent magnetization, $M(T)$ of the ITO nanostructure, Inset: Change in T_C with deposition pressure.

spectra, redshift of 363 cm^{-1} Raman mode shows the evidence of significant amount of V_O^+ formation within the ITO nanostructures. In addition, the inset of Fig. 7a shows a direct correlation between M_S and the corresponding PL blue emission (415 nm) intensity (I_B), which suggests that the V_O^+ defects are mainly responsible for such robust FM. In fact, the exact mechanism of the origin of ferromagnetism in such pure and doped oxides is not still very clear. However, several theoretical and experimental studies have shown that positively charged monovalent oxygen vacancy (V_O^+) near surface region is magnetic whereas it may be nonmagnetic within bulk of the oxides. Chang et al. [41] and Wang et al. [42] have shown that a magnetic triplet state is found to be the ground state of those defects in the vicinity of the SnO_2 surface, whereas the nonmagnetic singlet is the ground state of bulk SnO_2 . Here in our case for the ITO nanostructures, compared to other ITO morphologies, the nanowires have largest surface area, therefore containing more surface V_O^+ defects which give rise to strongest ferromagnetic ordering. Due to the loss of an O atom from ITO lattice, the electron pair that remains trapped in the oxygen vacancy cavity give rise to an F center defect [35]. One of the electrons in F center is likely to

occupy the neighboring In^{3+} ion and thus yields In^{2+} center and a F^+ center (V_O^+ defect) in the lattice [35]. The electron associated with such donor V_O^+ defect will be confined in an hydrogenic orbit [39] with radius, $r_H = \epsilon(m/m^*)a_0$, where ϵ is the high-frequency dielectric constant, m is the electron mass, m^* is the effective mass of the donor electrons and a_0 is the Bohr radius (53 pm). The magnetic moment ($\sim 1\ \mu_B$) of such trapped electron is localized at the center of the orbit [39]. As the concentration of oxygen vacancy defects increases in the specimen, more and more F^+ center orbit comes closer and finally overlap to other when the concentration exceeds a percolation threshold which can favor a long range ferromagnetic interaction [16,39]. Besides V_O^+ defects, a cation vacancy such as indium vacancy (V_{In}) here, can also induce significant magnetic moment which generally arises from the $2p$ orbital electrons of oxygen atom in the vicinity of V_{In} [6,7,15,40]. However, due to high formation energy, it is quite difficult to create and stabilize significant amount of V_{In} defects without any proper defect-engineering [35]. On the other hand, formation of V_O^+ defects is quite favorable especially when the ITOs are grown under an oxygen-deficient condition like here. Hence, as the NWs contain

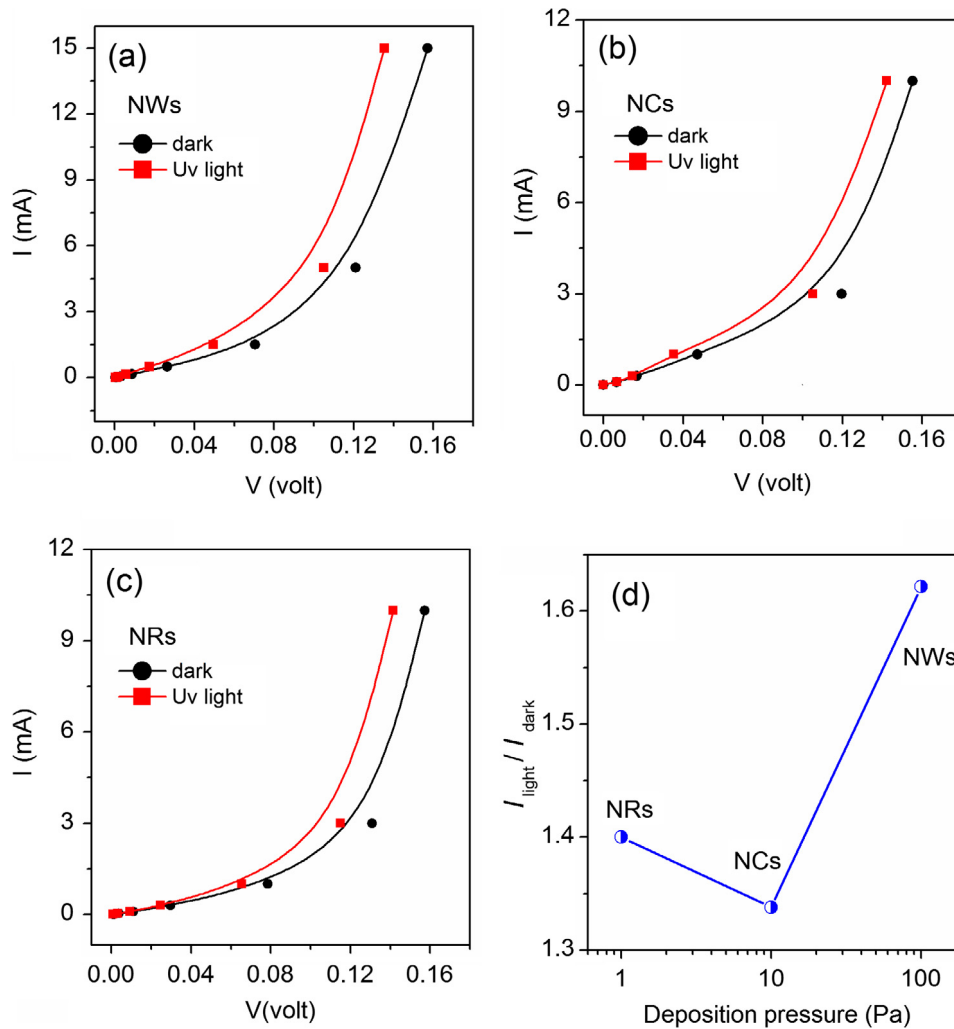


Fig. 8. Current voltage (I-V) characteristics for ITO (a) NWs, (b) NRs and (c) NCs under dark and UV-illumination. (d) The ratio of $I_{\text{light}}/I_{\text{dark}}$ are estimated at a constant voltage of 0.1 V for all the ITO nanostructures.

highest amount V_{O}^{\bullet} defects, it exhibits strongest FM as compared to the other morphologies.

3.6. I-V characteristics and photoresponse properties

Finally, the current-voltage (I-V) characteristics and photoresponse of ITO nanostructures is also investigated using ultraviolet (UV) light illumination. Fig. 8 shows the current-voltage (I-V) characteristics under dark and UV illumination for ITO (a) NWs, (b) NCs and (c) NRs of ITO. All the ITO nanostructures are found to exhibit non-ohmic (I-V) behavior demonstrating their semiconducting nature. In addition, it is quite interesting to notice that the current at a given voltage under UV-illumination is higher than under dark condition. This indicates that UV-illumination generates extra electron-hole pairs within the material which results in an increase in current. Thus, the effect of light on these nanostructures shows that the obtained 1D ITO nanostructures can be used as effective photovoltaic materials [43]. The ratio of $I_{\text{light}}/I_{\text{dark}}$ are estimated at a constant voltage of 0.1 V for all the ITO nanostructures. It can be seen from Fig. 8d that the ratio obtained for 1D nanostructures i.e. NWs and NRs are large compared to the comb-like nanostructures. This is because of large surface area of 1D NWs was exposed to the incident light and generates more electron-hole pair which contributes to the current. Hence, among the different

morphologies, defect-rich 1D NWs are found to be most photo-sensitive and thus can be used as promising photovoltaic material.

4. Conclusions

In conclusion, we have successfully fabricated one-dimensional (1D) indium-tin oxide nanostructures using pulsed laser deposition technique and investigated magnetic, optical, electrical and photoresponse properties in details. X-ray diffraction and field emission scanning electron microscopy (FESEM) revealed ITO possesses cubic bixbyite crystal structure of indium oxide with different nanostructure morphology like nanorods (NRs), nanocombs (NCs) and nanowires (NWs) for Ar pressure of 1, 10 and 100 Pascal (Pa) respectively. Evidence of oxygen-vacancy (V_{O}) formation within the lattice is confirmed from X-ray photoelectron, photoluminescence, Raman spectroscopic measurements. Photoluminescence spectra exhibited intense mid-band blue luminescence at wavelength of region of 400–450 nm due to the electronic transition from conduction band maxima (CBM) to the singly ionized oxygen-vacancy (V_{O}^{\bullet}) defect level within the band-gap. Oxygen vacancy in the ITO lattice is found to play a crucial role to determine the novel optical, electrical and magnetic properties. Due to presence of highest concentration of donor-type V_{O}^{\bullet} defects, the ITO NWs exhibited with high carrier (electron) concentration of

$\sim 6.4 \times 10^{20} \text{ cm}^{-3}$, low electrical resistivity. The ITO nanostructures also exhibited V_0^+ -mediated high- T_c ferromagnetism and the saturation magnetic moment (M_S) increases with increase of V_0^+ concentration. Current voltage (I-V) characteristics of ITO nanostructures showed an evidence of photo-induced current under UV illumination. Hence this study shows that such oxygen-deficient 1D ITO nanostructures can be used as promising materials for semiconductor spintronic, opto-electronic, and photovoltaic applications.

Acknowledgement

The authors acknowledge the support of Dr. U. Manju, CSIR-Central Glass and Ceramic Research Institute, Kolkata, India for the XPS measurements. The authors also thankful to Dr. Gautam Dev Mukherjee, Indian Institute of Science Education and Research, Kolkata for providing the micro-Raman spectrometer (LABRAM HR from Horiba Jobin Yvon) facility for measurements.

References

- [1] G.A. Prinz, *Magneto-electronics Sci.* 282 (1998) 1660–1663.
- [2] Y. Matsumoto, M. Murakami, T. Shono, T. Hasegawa, T. Fukumura, M. Kawasaki, P. Ahmet, T. Chikyow, S. Koshihara, H. Koinuma, Room-temperature ferromagnetism in transparent transition metal-doped titanium dioxide, *Science* 291 (2001) 854–856.
- [3] M. Venkatesan, C.B. Fitzgerald, J.M.D. Coey, Thin films: unexpected magnetism in a dielectric oxide, *Nature* 430 (2004) 630.
- [4] Hu. Shu-jun, Shi-shen Yan, Xue-ling Lin, Xin-xin Yao, Yan-xue Chen, Guo-lei Liu, Liang-mo Mei, Electronic structure of Fe-doped In_2O_3 magnetic semiconductor with oxygen vacancies: evidence for F-center mediated exchange interaction, *Appl. Phys. Lett.* 91 (2007) 262514.
- [5] S. Ghosh, D. De Munshi, K. Mandal, Paramagnetism in single-phase $\text{Sn}_{1-x}\text{Co}_x\text{O}_2$ dilute magnetic semiconductors, *J. Appl. Phys.* 107 (2010) 123919.
- [6] C.D. Pemmaraju, S. Sanvito, Ferromagnetism driven by intrinsic point defects in HfO_2 , *Phys. Rev. Lett.* 94 (2005) 217205.
- [7] I.S. Elfimov, S. Yunoki, G.A. Sawatzky, Possible path to a new class of ferromagnetic and half-metallic ferromagnetic materials, *Phys. Rev. Lett.* 89 (2002) 216403.
- [8] A. Sundaresan, R. Bhargavi, N. Rangarajan, U. Siddesh, C.N.R. Rao, Ferromagnetism as a universal feature of nanoparticles of the otherwise nonmagnetic oxides, *Phys. Rev. B* 74 (2006) 161306(R).
- [9] S. Ghosh, G.G. Khan, S. Varma, K. Mandal, Influence of Li-N and Li-F Co-Doping on Defect-Induced Intrinsic Ferromagnetic and Photoluminescence Properties of Arrays of ZnO Nanowires, *J. Appl. Phys.* 112 (2012) 043910.
- [10] S. Ghosh, G.G. Khan, K. Mandal, Defect-Driven Magnetism in Luminescent n/p-Type Pristine and Gd-Substituted SnO_2 Nanocrystalline Thin Films, *ACS Appl. Mater. Interfaces* 4 (2012) 2048–2056.
- [11] B. Santara, P.K. Giri, K. Imakitab, M. Fujiib, Evidence of oxygen vacancy induced room temperature ferromagnetism in solvothermally synthesized undoped TiO_2 nanoribbons, *Nanoscale* 5 (2013) 5476–5488.
- [12] M. Law, J. Goldberger, P. Yang, Semiconductor nanowires and nanotubes, *Ann. Rev. Mater. Res.* 34 (2004) 83–122.
- [13] C.N.R. Rao, F.L. Deepak, G. Gundiah, A. Govindaraj, Inorganic nanowires, *Prog. Sol. State Chem.* 31 (2003) 5–147.
- [14] A. Janotti, C.G. Van de Walle, Native point defects in ZnO, *Phys. Rev. B* 76 (2007) 165202–1–22.
- [15] S. Ghosh, G.G. Khan, B. Das, K. Mandal, Vacancy-Induced Intrinsic d^0 ferromagnetism and photoluminescence in potassium doped ZnO nanowires, *J. Appl. Phys.* 109 (2011) 123927–1–6.
- [16] A. Migani, G.N. Vayssilov, S.T. Bromley, F. Illas, K.M. Neyman, Dramatic reduction of the oxygen vacancy formation energy in ceria particles: a possible key to their remarkable reactivity at the nanoscale, *J. Mater. Chem.* 20 (2010) 10535–10546.
- [17] L.X. Guan, J.G. Tao, C.H.A. Huan, J.L. Kuo, L. Wang, Nonconventional magnetism in pristine and alkali doped In_2O_3 : density functional study, *J. Appl. Phys.* 108 (2010) 093911.
- [18] R. Podila, W. Queen, A. Nath, J.T. Arantes, A.L. Schoenhalz, A. Fazzio, G.M. Dalpian, J. He, S.J. Hwu, M.J. Skove, A.M. Rao, Origin of FM ordering in pristine micro- and nanostructured ZnO, *Nano Lett.* 10 (2010) 1383–1386.
- [19] G. Neri, A. Bonavita, G. Micali, G. Rizzo, F. Callone, G. Carturan, Resistive CO gas sensors based on In_2O_3 and InSnO_x nanopowders synthesized via starch-aided sol-gel process for automotive applications, *Sens. Actuators B* 132 (2008) 224–233.
- [20] B.G. Lewis, D.C. Paine, Applications and processing of transparent conducting oxides, *MRS Bull.* 25 (2000) 22–27.
- [21] J.C. Manificier, Thin metallic oxides as transparent conductors, *Thin Solid Films* 90 (1982) 297–308.
- [22] X.S. Peng, G.W. Meng, J. Zhang, X.F. Wang, Y.W. Wang, C.Z. Wang, L.D. Zhang, Synthesis and photoluminescence of single-crystalline In_2O_3 nanowires, *J. Mater. Chem.* 12 (2002) 1602–1605.
- [23] M. Kumar, V.N. Singh, F. Singh, K.V. Lakshmi, B.R. Mehta, J.P. Singh, On the origin of photoluminescence in indium oxide octahedron structures, *Appl. Phys. Lett.* 92 (2008) 171907.
- [24] J. Du, M. Yang, S.N. Cha, D. Rhen, M. Kang, D. Kang, Indium hydroxide and indium oxide nanospheres, nanoflowers, microcubes, and nanorods: synthesis and optical properties, *J. Crystal Growth Des.* 8 (2008) 2312–2317.
- [25] Y.Q. Chen, J. Jiang, B. Wang, J.G. Hou, Synthesis of tin-doped indium oxide nanowires by self-catalytic VLS growth, *J. Phys. D: Appl. Phys.* 37 (2004) 3319–3322.
- [26] G. Frank, L. Brock, H.D. Bausen, The solubilities of Sn in In_2O_3 and of In in SnO_2 crystals grown from Sn-In melts, *J. Cryst. Growth* 36 (1976) 179–180.
- [27] J. Ba, D.F. Rohlfing, A. Feldhoff, T. Brezesinski, I. Djerdj, M. Wark, M. Niederberger, Nonaqueous synthesis of uniform indium tin oxide nanocrystals and their electrical conductivity in dependence of the tin oxide concentration, *Chem. Mater.* 18 (2006) 2848–2854.
- [28] B.V. Crist, *Handbooks of Monochromatic XPS Spectra*, XPS International, 1997.
- [29] D. Maestre, A. Cremades, J. Piqueras, L. Gregoratti, Thermal growth and structural and optical characterization of Indium Tin Oxide nanopillars, nanoislands, and tubes, *J. Appl. Phys.* 103 (2008) 093531–1–6.
- [30] S.Y. Li, C.Y. Lee, P. Lin, T.Y. Tseng, Low temperature synthesized Sn doped indium oxide nanowires, *Nanotechnology* 16 (2005) 451–457.
- [31] J. Gao, R. Chen, D.H. Li, L. Jiang, J.C. Ye, X.C. Ma, X.D. Chen, Q.H. Xiong, H.D. Sun, T. Wu, UV light emitting transparent conducting tin-doped indium oxide (ITO) nanowires, *Nanotechnology* 22 (2011) 195706–1–22.
- [32] H. Cao, X. Qiu, Y. Liang, Q. Zhu, M. Zhao, Room-temperature ultraviolet-emitting In_2O_3 nanowires, *Appl. Phys. Lett.* 83 (2003) 761–763.
- [33] C.L. Hsin, J.H. He, L.J. Chen, Modulation of photoemission spectra of In_2O_3 nanowires by the variation in Zn doping level, *Appl. Phys. Lett.* 88 (2006) 063111–1–3.
- [34] M. Seetha, P. Meena, D. Mangalaraj, Y. Masuda, K. Senthil, Synthesis of indium oxide cubic crystals by modified hydrothermal route for application in room-temperature, *Mater. Chem. Phys.* 133 (2012) 47–54.
- [35] N. Serpone, Is the band gap of pristine TiO_2 narrowed by anion- and cation-doping of titanium dioxide in second-generation photocatalysts?, *J. Phys. Chem. B* 110 (2006) 24287–24293.
- [36] J. Gan, X. Lu, J. Wu, S. Xie, T. Zhai, M. Yu, Z. Zhang, Y. Mao, S.C.I. Wang, Y. Shen, Y. Tong, Oxygen vacancies promoting photoelectrochemical performance of In_2O_3 nanocubes, *Sci Rep.* 3 (2013) 1021.
- [37] Ç. Kiliç, A. Zunger, Origins of coexistence of conductivity and transparency in SnO_2 , *Phys. Rev. Lett.* 88 (2002) 095501–1–4.
- [38] X. Du, Y. Du, S.M. George, In situ examination of tin oxide atomic layer deposition using quartz crystal microbalance and Fourier transform infrared techniques, *J. Vac. Sci. Technol. A* 23 (2005) 581–588.
- [39] J.M.D. Coey, M. Venkatesan, C.B. Fitzgerald, Donor impurity band exchange in dilute ferromagnetic oxides, *Nat. Mater.* 4 (2005) 173–179.
- [40] G. Bouzerar, T. Ziman, Model for vacancy-induced d^0 ferromagnetism in oxide compounds, *Phys. Rev. Lett.* 96 (2006) 207602–207605.
- [41] G.S. Chang, J. Forrest, E.Z. Kurmaev, A.N. Morozovska, M.D. Glinchuk, J.A. McLeod, A. Moewes, T.P. Surkova, Nguyen Hoa Hong, Oxygen-vacancy-induced ferromagnetism in undoped SnO_2 thin films, *Phys. Rev. B* 85 (2012) 165319–1–5.
- [42] H. Wang, Y. Yan, K. Li, X. Du, Z. Lan, H. Jin, Role of intrinsic defects in ferromagnetism of SnO_2 : first-principles calculations, *Phys. Stat. Sol. (b)* 247 (2010) 444–448.
- [43] M.N. Borah, S. Chaliha, P.C. Sarmah, A. Rahman, Studies on current-voltage characteristics of ITO/(n) CdSe-Al heterojunctions, *J. Optoelectron. Adv. Mater.* 10 (2008) 2793–2799.